
CONSTRAINED PLASTICITY RESERVE AS A NATURAL WAY TO CONTROL FREQUENCY AND WEIGHTS IN SPIKING NEURAL NETWORKS

A PREPRINT

Oleg Nikitin
Computing Center
Far Eastern Branch
Russian Academy of Sciences
680000, Khabarovsk, Russia
olegioner@gmail.com

Olga Lukyanova*
Computing Center
Far Eastern Branch
Russian Academy of Sciences
680000, Khabarovsk, Russia
ollukyan@gmail.com

Alex Kunin
Computing Center
Far Eastern Branch
Russian Academy of Sciences
680000, Khabarovsk, Russia
alexxkunin88@gmail.com

March 30, 2024

ABSTRACT

Biological neurons have adaptive nature and perform complex computations involving the filtering of redundant information. Such processing is often associated with Bayesian inference. Yet most common models of neural cells, including biologically plausible, such as Hodgkin-Huxley or Izhikevich do not possess predictive dynamics on the level of a single cell. The modern rules of synaptic plasticity or interconnections weights adaptation also do not provide grounding for the ability of neurons to adapt to the ever-changing input signal intensity. While natural neuron synaptic growth is precisely controlled and restricted by protein supply and recycling, weight correction rules such as widely used STDP are efficiently unlimited in change rate and scale. In the present article, we will introduce new mechanics of interconnection between neuron firing rate homeostasis and weight change by means of STDP growth bounded by abstract protein reserve, controlled by the intracellular optimization algorithm. We will show, how these cellular dynamics help neurons to filter out the intense signals to help neurons keep a stable firing rate. We will also examine that such filtering does not affect the ability of neurons to recognize the correlated inputs in unsupervised mode. Such an approach might be used in the machine learning domain to improve the robustness of AI systems.

Keywords Neural homeostasis · Spike-timing-dependent plasticity · Synaptic scaling · Adaptive control · Bio-inspired cognitive architectures

1 Motivation

Modern neural networks and deep learning systems still lack the generalization and self-learning abilities of natural brains. Also, deep neural nets (DNN) need a lot of labeled data. Being tuned for one particular task and dataset DNNs may not perform so well in real practical application. These are major obstructions in the widespread implementation of deep learning systems for practical use [1]. Spiking neural nets (SNN) train in unsupervised setup and doing well in the data generalization. Yet, training of SNN still needs to be improved to be widely used. In the present article, we propose to include some features of cellular self-organization into the spike-timing-dependent (STDP) weight update rule [2] to improve the ability of SNN to process the dynamic input signals.

Biological cells do possess a molecular and genetic substrate for complex adaptation and regulation and perform different kinds of actions and decisions to act adaptively in the dynamic environment. Such adaptive structures present as *genetic regulatory networks* (GRN) and *protein-protein interaction* (PPI) networks [3] that can be viewed as reservoir computer [4]. (Figure 1)

*Corresponding author

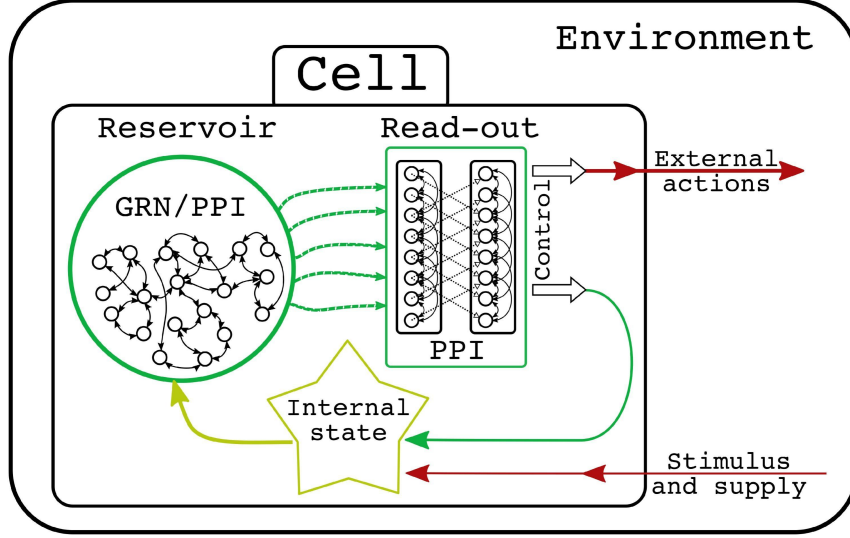


Figure 1: The conceptual structure of a biological cell as reservoir computing device.

Reservoir computer (RC) represents a unified concept for uniting different kinds of recurrent neural networks, drawing inspiration from the natural systems. In RC systems only the readout layer of the network is trainable while the weights of other parts of the network are fixed and randomly assigned [5]. Such a feature of RC makes it a good abstraction for complex networks of biological cells [4, 6], in which some nodes of the interaction graph (such as the interplay between genes and transcriptions) are fixed and other nodes can be tuned to the dynamical situations. The most notable kinds of reservoir computing are *liquid state machines* (LSM) [7] and *echo state networks* (ESN) [8]. For example, GRN and PPI networks of *Escherichia coli* were modeled in several studies [4, 6, 9] and even genetically modified to create a reservoir computer in the wet lab [10].

Human GRN and PPI are much more complicated than those from simple prokaryotic organism *E.coli* and provide much more computational power. Sinha et al. [11] propose to consider behavior-related GRNs as a basic layer of organization of neural networks in the brain. In the present article, we view GRNs and PPIs as an abstract reservoir computing device that allows cells, including neurons, to perform the intelligence tasks on an intracellular basis.

Neurons perform adaptive rapid and long-lasting learning. Now in modeling, most of that learning abilities are referred only to the change in the efficiency of connections between the cells. Intracellular control and complexity are neglected in the simulations, while the inclusion of some cellular adaptivity might be beneficial for robust AI systems. Below we propose to include some cellular control into the plasticity algorithms of neural networks.

The regulation of synaptic strength and membrane excitability plays a crucial role in learning and memory in biological neural networks. These are complex processes involving a huge network of genetic messengers such as *mRNA* and complex interactions of proteins. Such complex control networks stretch from cellular nucleus to membrane and may perform a surprisingly complex behavior.

For example, it was shown, that individual Purkinje cells may learn a complex response to the unconditioned stimulus. (Figure 2) This is expressed as delayed silencing of intrinsic action potential (AP) generation in response to particular excitatory inputs [12]. This process functions by the pairing of the unconditioned stimulus, which leads to the hyperpolarization of the membrane and delayed conditioned stimulus. As a result, conditioned stimulus alone leads to the opening of *Kir3* potassium channels with some delay and hyperpolarization of the cell membrane and silencing of the AP generation of the cell [13].

It is remarkable in the described phenomenon that one neuron, not the assembly of cells may be a substrate to classical conditioning. According to this study, the single cell may learn to inhibit its activity with learned delay time in response to a previous excitatory stimulus. This outstanding ability of Purkinje Cells is probably based on the intracellular interaction between the *mGluR7* receptors of glutamate, an excitatory neurotransmitter, and microtubules, forming cytoskeleton. Microtubules do adapt in response to *mGluR7* stimulus to form the precise delays in the *Kir3* activation. Such intracellular apparatus was found not only in Purkinje cells but also in striatal medium spiny neurons. Such complex networks may exist in all neurons and may control different complex responses and functions. For the first time to our knowledge, conditioned stimulus on the isolated neuron was found in [14].

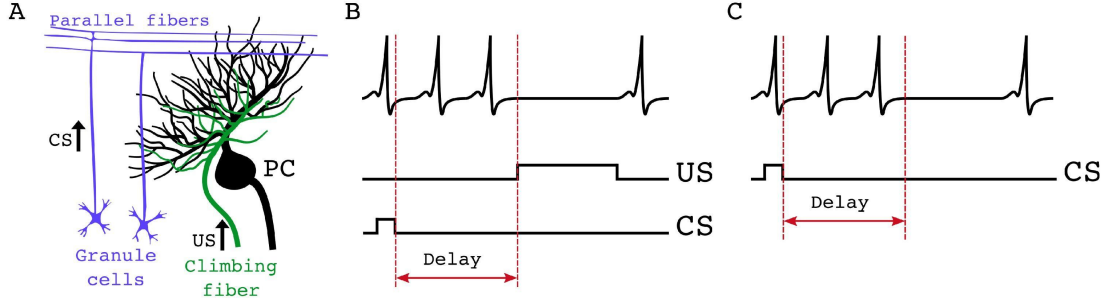


Figure 2: Conditioned learning of pause response in spontaneous activity of Purkinje cell. (A) A simplified structure of cellular interactions in the model system. Axons growing from inferior olive is called climbing fiber (CF) act as an unconditioned stimulus (US, green). Axons of granule cells called parallel fibers (PF) act as a conditioned stimulus (CS, violet). Purkinje cell itself is showed black and marked as PC. (B) PC response on stimulation via CF and PF before the learning of US pairing. Cell response is shown on the top. It can be seen that stimulation with the US causes the stop of spiking and the CS delivered with some delay before the US. (C) PC response after the learning of conditioned response. PC interrupts spiking with precise delay in response to CS (stimulation of PF) alone.

Molecular networks governing the synapse functioning are not less complex than those controlling the membrane responsibility [15, 16]. Multiple proteins and genetic carriers play role in the formation of long-term potentiation (LTP) and memory. In a biological cell, synapse should be initiated, grown, and maintained to form the memory. Synaptic plasticity itself is very much dependent on the expression of neurotransmitter receptors upon the cellular membrane. There are many types of neurotransmitters and receptors to read them as cellular signals. But we believe they all have some kind of 'intracellular machine' that control their dynamics to let cell perform its function and to keep integrity on the way.

We will focus on the example of glutamate transmission, as it is best studied among other ways of neurochemical signaling. The glutamate transmission is intermediated mostly by AMPA and NDMA types of receptors. These receptors are protein molecules that have to be secreted by *endoplasmatic reticulum* (ER) and then transported to the postsynaptic membrane, kept on the surface of the cell, and degraded when needed. All the steps of this process are precisely tuned and adaptively controlled by complex molecular interactions. Receptors are assembled and synthesized in the ER and then incorporated into the vesicles for export. Dendritic ER can vary the rate of receptor transport to synapses, depending on the level of intracellular calcium. LTD mechanism can use regulation of receptor traffic from ER, mediated via transmembrane AMPA receptor regulatory proteins such as stargazin [17]. Reticulons like *Nogo-A* also play role in the activity-dependent regulation of receptor trafficking and secretion [18, 19, 20]. Protein kinases, such as *PKM ζ* or *PKC λ* play role in keeping induced LTP long-term stability [21, 22]. In general, most signaling pathways are interconnected with cellular transcription factor proteins of CREB class, which, in turn, is Ca^{2+} ion-dependent [23]. The amount of CREB proteins, stored in the ER pool determines the ability of synapses to learn and the neuronal competition during memory formation [24].

Any living cell, in general, has to perform allostasis as a process of predictive regulation of the cellular state in order to survive in the future in the dynamic environment [25]. For neurons as for excitable cells, the most important marker of persistent activity is Ca^{2+} ions and the level of calcium in the soma might be interpreted as a function from the frequency of membrane excitation [26]. In all kinds of living cells, the level of Ca^{2+} is a key part of cellular signaling and control [27].

We propose, that all the processes described above might be generalized into a more abstract representation. Neurons should keep their firing frequency (or cytoplasmic Ca^{2+} level) on a more or less constant level and regulate against overexcitation. This is done by predictive up or downregulation of different sources of proteins, which allow cells to let in more or less extracellular excitatory or inhibitory stimulus. (Figure 3)

We would like to proceed by the way proposed in [1], or building less 'artificial' neural networks with some bio-inspiration. We use the spiking neuron model not only because it is biologically more plausible but also because it has some meaningful advantages. Spiking neural nets are efficient in terms of energy consumption and memory allocation, better suited for sequential data processing, than regular neural nets [28]. Spiking neurons might be a good model for the implementation of predictive learning approaches [29]. With regular networks with backpropagation, it is hard to implement recurrent architectures [30]. Most importantly, 'traditional' artificial neural network (ANN) may act only reactive towards input signals.

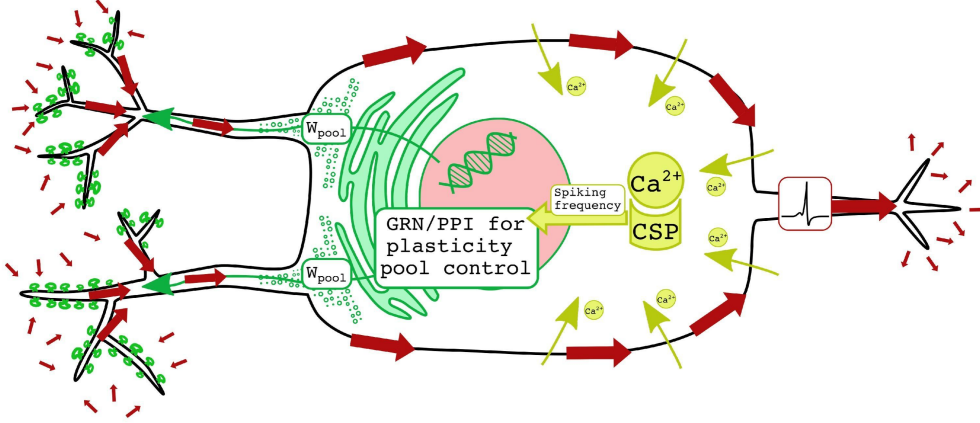


Figure 3: Conceptual representation of a neuron with weight growth materials control. Red arrows depict the input currents, yellow – represent calcium influx, green – weight change ‘materials’ flow going from the ‘materials’ synthesis and control structures. CSP is calcium-sensing proteins providing information about the level of calcium influx, and thus representing current spiking frequency, to weight ‘materials’ control structures.

Despite the advantages of spiking nets, they are not well suited for backpropagation algorithms due to the non-differentiable nature of the signals in the network. At the same time, Hebbian learning [31] approaches such as STDP provide suitable rules for local unsupervised learning. STDP type of learning is well studied and it is good at finding coincidences in the data [2]. It was shown that STDP only rule with no constraints will lead to runaway activity [32]. It was found that biological synapses are constrained by homeostatic scaling [33] when all the weights are dynamically rescaled to form the constant ‘sum’ of synaptic weights on the same region of the neuron and to keep the proportion of synaptic weights. Also, heterosynaptic scaling exists [34], when growth (or long term potentiation, LTP) of one synapse leads to a decrease (or long term depression, LTD) of other synapses. Both processes are very important for the stability and reliable work of natural neural systems.

The computational model of homeostatic synaptic scaling was first introduced in [35]. Zenke et al. [36] demonstrated that homeostatic synaptic scaling alone would lead to unstable behavior of networks and that STDP weight growth should be constrained by frequency-dependent regulation (Figure 4A). At the same time, in [36], mechanics leading to heterosynaptic scaling is not provided. (Figure 4B) A computational model of weight restraining rule leading to the heterosynaptic regulation was proposed in [32, 37]. It was implemented basically as homeostatic synaptic scaling that works only for most extreme (small or big) weights and only when the firing frequency of a neuron is too high. This prevents neurons from runaway activity and leads to the potentiation of some synapses against another. But it is unclear from the model if it preserves the most correlated and important connections.

Contemporary neural systems, both based on backpropagation or forms of Hebbian learning, potentially allow unconstrained weight growth and it should be artificially restricted. But restrictions such as scaling do affect long-term standing memories and it is hard to answer, how some connections in brains maintain stability for decades despite constant rescaling. In this paper, we would like to investigate a new bio-inspired rule for the control of synaptic growth in the STDP model and its learning stability and ability to recognize correlations in the input information.

Natural synaptic weight growth is tightly constrained by construction ‘materials’ (proteins) availability and precisely controlled in respect to maintaining stable cellular activity [38, 39]. Below, we propose the model, which naturally regulates the weight growth in all the parts of the compartmentalized artificial neural cell via the control of the storage of reserve of abstract ‘materials’ for potential synaptic weight growth. Weight growth in all the parts of such compartmentalized artificial neural cells is restricted via the control of the availability of ‘materials’ for potential synaptic weight growth. This type of restriction is non-linear and may naturally regularize the growth of weights in the STDP rule.

2 Methods

The basic STDP rule does not provide some features of learning and adaptivity that are typical for natural learning systems. Also, STDP is hard to train in a supervised setup. In the current paper, we propose the novel model of control

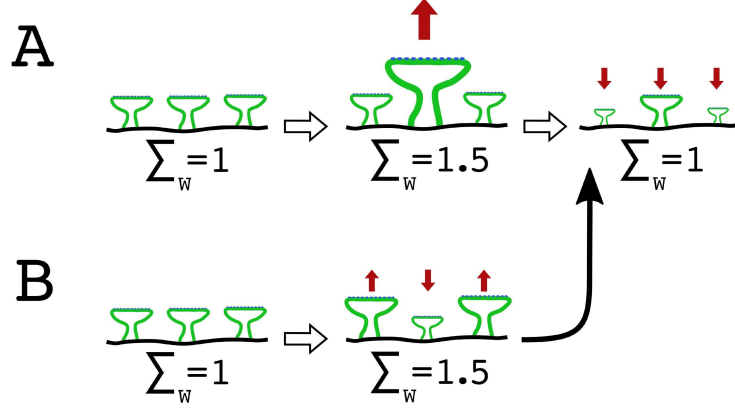


Figure 4: Synaptic connections dynamics during processes of: (A) homeostatic synaptic scaling, (B) heterosynaptic scaling. On (A), the growth of one synapse is then compensated by decreasing all synapses sizes to maintain the stable 'sum' of all connections weights in a particular region of a dendrite. The timescale of the process is quite long and may last for hours. On (B), extensive growth of most synapses in one area leads to instant shrinkage of the less stimulated synapses. This process is not keeping the 'sum' of synapses constant and may be continued by (A).

of STDP weights, which will improve its ability to learn and in the future may provide grounding for different learning setups, including semi-supervised.

This work is a continuation of previous research on activity homeostasis in neural networks [40], where authors proposed a model of a neural cell, which allows switching behavioral programs, maintaining a stable cell functioning, and responding to changes in the dynamics of input signals. The most important processes of adaptive correction of neuronal activity were considered: synaptic plasticity, regulation of intracellular dynamics of transport and secretion of neuromodulator receptors, as well as the adaptive functioning of intracellular regulatory networks. Approaches to modeling the basic properties of these processes were discussed in detail in [40]. A homeostatic neuron model with dependent input-switching activity was shown in [41] and was studied the properties of homeostasis and switching based on the frequency homeostasis.

Based on the research discussed above, we propose the neuronal plasticity regulation model, which changes the potential synaptic weight growth by the control of the plasticity potential reserve to dynamically stabilize the artificial neuron activity. We introduce the concept of 'plasticity potential reserve' as generalized abstract 'materials' for the potential growth of synaptic weight in our model. It is used to regulate the processes in the cell.

We will use a model of one spiking neuron with dendrites and an activation model based on [42].

We will consider neuron n with m synaptic inputs distributed across d dendritic compartments such that each dendrite has s synapses. As we consider only one neuron we can discard n term and operate only with m weights w_m across d dendrites. Furtherly we uniquely map w_{nm} to w_{ds} . So, we define w_{ds} as a current synaptic weight of the synapse s on the dendrite d in time t . All weighted inputs are collected first at dendrites d and the signals from dendrites are collected on the somatic body of the neuron and projected to the activity of the Izhikevich model. Below, we will cover the basic model dynamics and the model of constrained growth of STDP weights.

2.1 Spike-timing-dependent plasticity (STDP)

The STDP model describes the change in synaptic weight as a function of the delay between the timing of the release of spikes by presynaptic and postsynaptic neurons. We denote Δw_{ds}^{stdp} as an update of the synaptic weight of the synapse s on the dendrite d , according to the model, introduced in [43]:

$$\Delta w_{ds}^{stdp} = \begin{cases} A_+(w_{ds}) \cdot \exp(-\Delta t / \tau_+), & \text{if } \Delta t \geq 0, \\ -A_-(w_{ds}) \cdot \exp(\Delta t / \tau_-), & \text{if } \Delta t < 0, \end{cases} \quad (1)$$

where Δw_{ds}^{stdp} is the update of the synaptic weights by STDP rule; $\Delta t = t_{sp}^{(pre)} - t_{sp}^{(post)}$ is the interval between the occurrence of subsequent spikes at presynaptic and postsynaptic neurons; τ_+ and τ_- is the characteristic time defining a time interval, which may cause successful correlation effects; $A_+(w_{ds})$ and $A_-(w_{ds})$ are the coefficients that reflect the maximum possible rate of change of synaptic weights w_{ds} and may depend upon its current value.

To ensure that the synaptic weights do not take abnormal values during the dynamics of the neural network, the interval $w_{min} < w_{ds} < w_{max}$ of their admissible values is usually introduced and, respectively, the functions $A_+(w_{ds})$ and $A_-(w_{ds})$ are defined as follows:

$$\begin{aligned} A_+(w_{ds}) &= (w_{max} - w_{ds}) \cdot A_+, \\ A_-(w_{ds}) &= (w_{ds} - w_{min}) \cdot A_-, \end{aligned} \quad (2)$$

where A_+ and A_- are the positive parameters.

Here, in our model: $A_+ = 0.25$, $A_- = 0.25$, $w_{max} = 1.0$, $w_{min} = 0.0$, $\tau_+ = 10$, $\tau_- = 10$.

2.2 Input scaling and output model

For calculating the spiking O of the neuron we use a model of spiking neurons proposed by Izhikevich [42]:

$$\begin{aligned} \dot{v} &= 0.04v^2 + 5v + 140 - u + I, \\ \dot{u} &= a(bv - u) \end{aligned} \quad (3)$$

with the auxiliary after-spike resetting

$$\text{if } v \geq v_{peak}, \text{ then } \begin{cases} v \leftarrow c \\ u \leftarrow u + d \end{cases} \quad (4)$$

where v is the membrane potential of the neuron, u is the membrane recovery variable, which accounts for the activation of K^+ ionic currents and inactivation of Na^+ ionic currents, and it provides negative feedback to v ; I is the input current; a is the time scale of the recovery variable u ; b is the sensitivity of the recovery variable u to the subthreshold fluctuations of the membrane potential v ; c is the after-spike reset value of the membrane potential v caused by the fast high-threshold K^+ conductances; and d is the after-spike reset of the recovery variable u caused by slow high-threshold Na^+ and K^+ conductances.

After the spike reaches its apex v_{peak} , the membrane voltage and the recovery variable are reset according to the Equation 4. Synaptic currents or injected dc-currents are delivered via the variable.

Here, the input current I is the sum of all the received inputs I_{ds} to each synapse s on the dendrite d multiplied by all synaptic weights w_{ds} , respectively. It is averaged over synapses and then over dendrites and scaled by the input scaling coefficient:

$$I = \frac{1}{D} \cdot \sum_d \left(\frac{2 \cdot \sum_s (I_{ds} \cdot w_{ds})}{S \cdot (w_{max} - w_{min})} \right) \cdot k^{izh}, \quad (5)$$

where w_{max} and w_{min} are the maximum and the minimum possible weights from the Equation 2; S is the number of synapses on each dendrite; D is the number of dendrites; k^{izh} is the input scaling coefficient,

$$k^{izh} = (1 + b) \cdot v_{peak} + \frac{d}{a} - 0.08c^2 + (b - 11) \cdot c - 280 \quad (6)$$

where a , b , c , d , v_{peak} are the same parameters that are presented in the Equations 3–4.

The Equation 6 was obtained by searching for such a state according to the Equation 3 so that with average weights between the maximum w_{max} and the minimum w_{min} , and the frequency of inputs θ_{input} equal to 0.5, the firing frequency θ_{real} was also equal to 0.5. This scaling coefficient is used to adapt the input to Izhikevich model to allow the firing frequency variation necessary for our experiments.

Along with checking by the Equation 4 whether the value of the neuron membrane potential v has exceeded the peak value v_{peak} , the output from the action potential generation model (3–6) O is also calculated each step for all neuron as follows:

$$O = \begin{cases} 0, & \text{if } v < v_{peak} \\ 1, & \text{if } v \geq v_{peak} \end{cases} \quad (7)$$

So, if v exceeds v_{peak} then the action potential generation (spiking) O is occurring.

In our model the parameters of the spiking neuron model were as follows: $a = 0.02$, $b = 0.23$, $c = -65.0$, $d = 2.00$, $v_{peak} = 20$ mV.

Above we specified an overall setup of our basic neuron and plasticity model. This is a common Izhikevich spiking neuron with the STDP plasticity model. The goal of this article is to study frequency-dependent constraints for the STDP weight growth. Below, we will first describe our implementation of homeostatic synaptic plasticity. Then, we will introduce a novel model of plasticity restriction arising from the phenomena of natural limits of resources available for weight growth. We call it the plasticity potential reserve control model.

2.3 Homeostatic synaptic scaling (HSS)

Here, we implement a simple version of an approach to homeostatic synaptic plasticity described in [35]. The basic idea is to scale all weights of a neuron in response to firing frequency changes.

After adding Δw_{ds}^{stdp} , synaptic weights w_{ds} are corrected depending on the deviation of spiking frequency from the target:

$$\dot{w}_{ds} = k_d^{hss} \cdot (w_{ds} + \Delta w_{ds}^{stdp}), \quad (8)$$

where k^{hss} is the HSS correction coefficient,

$$k^{hss} = 1 - (\theta_{real} - \theta_{target}), \quad (9)$$

where θ_{real} is the current firing frequency and θ_{target} is the target firing frequency.

Here, θ_{target} is a given target constant and θ_{real} is a simple moving average (SMA) calculated as:

$$\theta_{real} = \frac{\sum_{t=wind}^t O(t)}{wind} \quad (10)$$

where $O(t)$ is the action potential generation (spiking) at the time t , which can be '0' or '1', and $wind$ is the given window, showing how many steps back we are looking.

The further the value of the θ_{real} is from the value of the θ_{target} , the proportionally this decreases Δw_{ds}^{stdp} in the directions that can increase the difference between these frequencies. Thus, this rule holds back the distance between 'real' and 'target' firing frequencies.

The presented homeostatic synaptic scaling approach set a linear restriction on all the input weights. While for efficient learning it is beneficial to reinforce the most important signals and to filter an effective noise. In the next section, we describe the non-linear dynamic approach to weight outgrowth control.

2.4 Nonlinear constrained STDP

As we described above in the Section 1 of the paper, biological neurons do control the weight growth and firing frequency by complex intracellular GRN/PPI networks. Below, we introduce an abstract model of such a control approach, based on the availability of abstract 'materials' required for the weight growth. The present approach allows for natural competition between synapses on dendrites and competition between different dendrites. The model schematically showed in Figure 5.

Three main parts of the system are following:

1. the reserve of synaptic weight growth in the soma (w_{soma}^{pool}) and in dendrites (w_d^{pool});
2. action potential generation model (spiking model) and firing frequency detector;
3. update algorithm for the reserve of synaptic weight growth with regard to firing frequency control.

The reserve of synaptic weight growth moves unidirectionally from the soma to dendrites. In the dendrites, the growth materials are used during LTP and partly returned to dendrite during LTD. The particular implementation of the control algorithm might be different ranging from simple frequency dependant control or some kind of black box control system or the differential equations for optimal control.

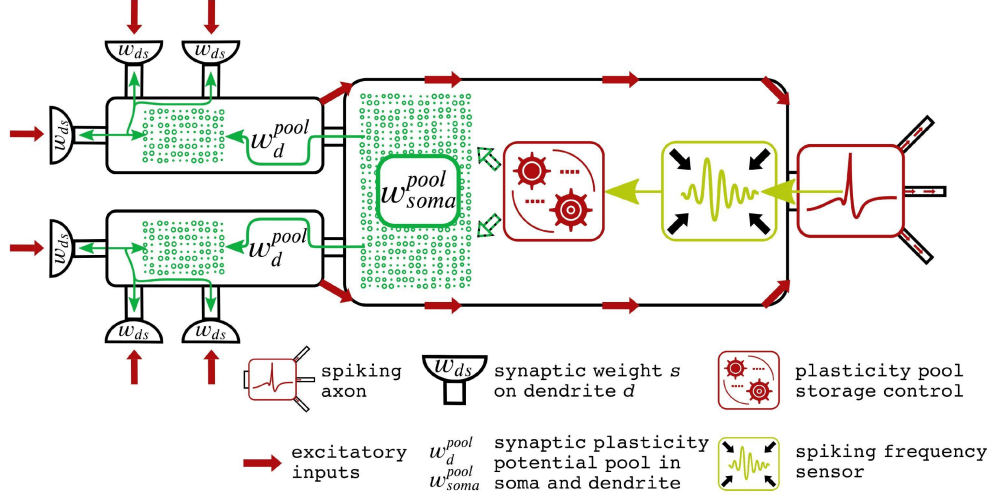


Figure 5: Schematic representation of proposed weight control model.

2.4.1 Weights dynamics restrictions

Below, we describe the additions and extensions to STDP that introduce some non-linearity and weight growth control. Consider the dynamics of the synaptic weights w_{ds} by the dendrite d and synapse s respectively:

$$\dot{w}_{ds} = k_d^{siss} \cdot (w_{ds} + \Delta w_{ds}^{stdp}), \quad (11)$$

where \dot{w}_{ds} is the dynamics in the synaptic weight of the synapse s on the dendrite d with respect to time; k_d^{siss} is the spike-independent synaptic scaling coefficient on the dendrite d ; w_{ds} is the current synaptic weight of the synapse s on the dendrite d in time t ; Δw_{ds}^{stdp} is the update of the synaptic weights by spike-timing-dependent plasticity of the synapse s on the dendrite d .

Here, we distinguish two processes of weight dynamics depending on the plasticity potential:

1. Plasticity potential constraints for STDP

We add restriction coefficient of the synaptic weight growth k_d^{wp} :

$$\Delta w_{ds}^{stdp} = \begin{cases} \Delta w_{ds}^{stdp}, & \text{if } \Delta w_{ds}^{stdp} < 0, \\ k_d^{wp} \cdot \Delta w_{ds}^{stdp}, & \text{if } \Delta w_{ds}^{stdp} > 0, \end{cases} \quad (12)$$

where k_d^{wp} is the restriction coefficient of the growth of synaptic weights depending on the deviation from the optimum frequency.

$$k_d^{wp} = 1 + \left(\frac{w_d^{pool}}{k_d^{siss} \cdot \sum_s \Delta w_{ds}^{stdp+}} - 1 \right) \cdot H \left(\sum_s \Delta w_{ds}^{stdp+} - \frac{w_d^{pool}}{k_d^{siss}} \right) \quad (13)$$

where w_d^{pool} is the potential reserve of synaptic weight growth on the dendrite d ; $\sum_s \Delta w_{ds}^{stdp+}$ is the sum by the synapse s of all positive STDP updates of the synaptic weights, and $\sum_s \Delta w_{ds}^{stdp+} = \sum_s (k_d^{wp} \cdot \Delta w_{ds}^{stdp})$,

where $\Delta w_{ds}^{stdp} > 0$; $H\left(\sum_s \Delta w_{ds}^{stdp} - \frac{w_d^{pool}}{k_d^{siSS}}\right)$ is a Heaviside step function $H(x)$, also known as the 'unit step function', and written as

$$H(x) = \begin{cases} 0, & \text{if } x < 0 \\ 1, & \text{if } x > 0 \end{cases} \quad (14)$$

2. Spike-independent synaptic scaling (SISS)

Gonzalez-Islas et al. [44] and Fong et al. [45] have shown that synaptic stabilization is performed in postsynaptic local compartments independent from the firing frequency, despite the model of Van Rossum et al. [35]. Here we perform spike-independent synaptic scaling (SISS) on dendritic branches. This means that the sum of all weights on one particular dendrite is aimed to be constant. We set a goal weight w_{ds}^{ideal} for each particular synapse and then calculate the scaling coefficient for all synapses on the dendrite according to the Equation 15:

$$k_d^{siSS} = 1 - r^{siSS} \cdot \left(1 - \frac{\sum_s w_{ds}^{ideal}}{\sum_s w_{ds}}\right), \quad (15)$$

where w_{ds}^{ideal} is the target specified sum of the synaptic weights of the dendrite d ; and r^{siSS} is the rate coefficient, shows how many steps the weight should take to reach the w_{ds}^{ideal} ,

$$r^{siSS} = \frac{1}{t_{step}^{ideal}} \quad (16)$$

Thus, the dynamics of synaptic weights are calculated using the processes of weight dynamics depending on the plasticity potential (STDP and SISS), which have different effects on the resulting value of synaptic weights (increase or decrease), and determines the potential reserve of synaptic weight growth.

2.4.2 Plasticity potential reserve dynamics

So, we can calculate the dynamics of the plasticity potential reserve of synaptic weight growth on the dendrite d using the following equation:

$$\dot{w}_d^{pool} = w_d^{pool} - \sum_s \Delta w_{ds}^- - k_d^{sat} \cdot \sum_s \Delta w_{ds}^+ + k_{soma}^{sat} \cdot r^{speed} \cdot \Delta w_d^{pool} \quad (17)$$

where Δw_{ds}^- are the weights returned back to the plasticity potential reserve of synaptic weight growth on the dendrite d for the growth of weights at s synapses; Δw_{ds}^+ are the weights consumed from the plasticity potential reserve of synaptic weight growth on the dendrite d for the growth of weights at s synapses; k_d^{sat} is the coefficient showing the sufficiency of the plasticity potential reserve of synaptic weight growth to satisfy the amplitude of the growth in all weights on the dendrite d ; Δw_d^{pool} is the demand on the replenishment of the potential reserve of synaptic weight growth w_d^{pool} up to maximum amplitude of growth of the sum of weights w_d^{res} ; r^{speed} is the transfer speed coefficient; and k_{soma}^{sat} is the coefficient showing the sufficiency of the plasticity potential reserve of synaptic weight growth to satisfy the amplitude of the growth in all weights on the soma.

$$\Delta w_{ds}^- = k_{back} \cdot (\dot{w}_{ds} - w_{ds}) \cdot (1 - H(\Delta w_{ds})) \quad (18)$$

where k_{back} is the return coefficient of excess changes in synaptic weights to the potential reserve.

$$\Delta w_{ds}^+ = (\dot{w}_{ds} - w_{ds}) \cdot H(\Delta w_{ds}), \quad (19)$$

$$k_d^{sat} = 1 + \left(\frac{w_d^{pool}}{\sum_s \Delta w_{ds}^+} - 1\right) \cdot H\left(\sum_s \Delta w_{ds}^+ - w_d^{pool}\right) \quad (20)$$

$$\Delta w_d^{pool} = (w_d^{res} - w_d^{pool}) \cdot H(\Delta w_d^{pool}), \quad (21)$$

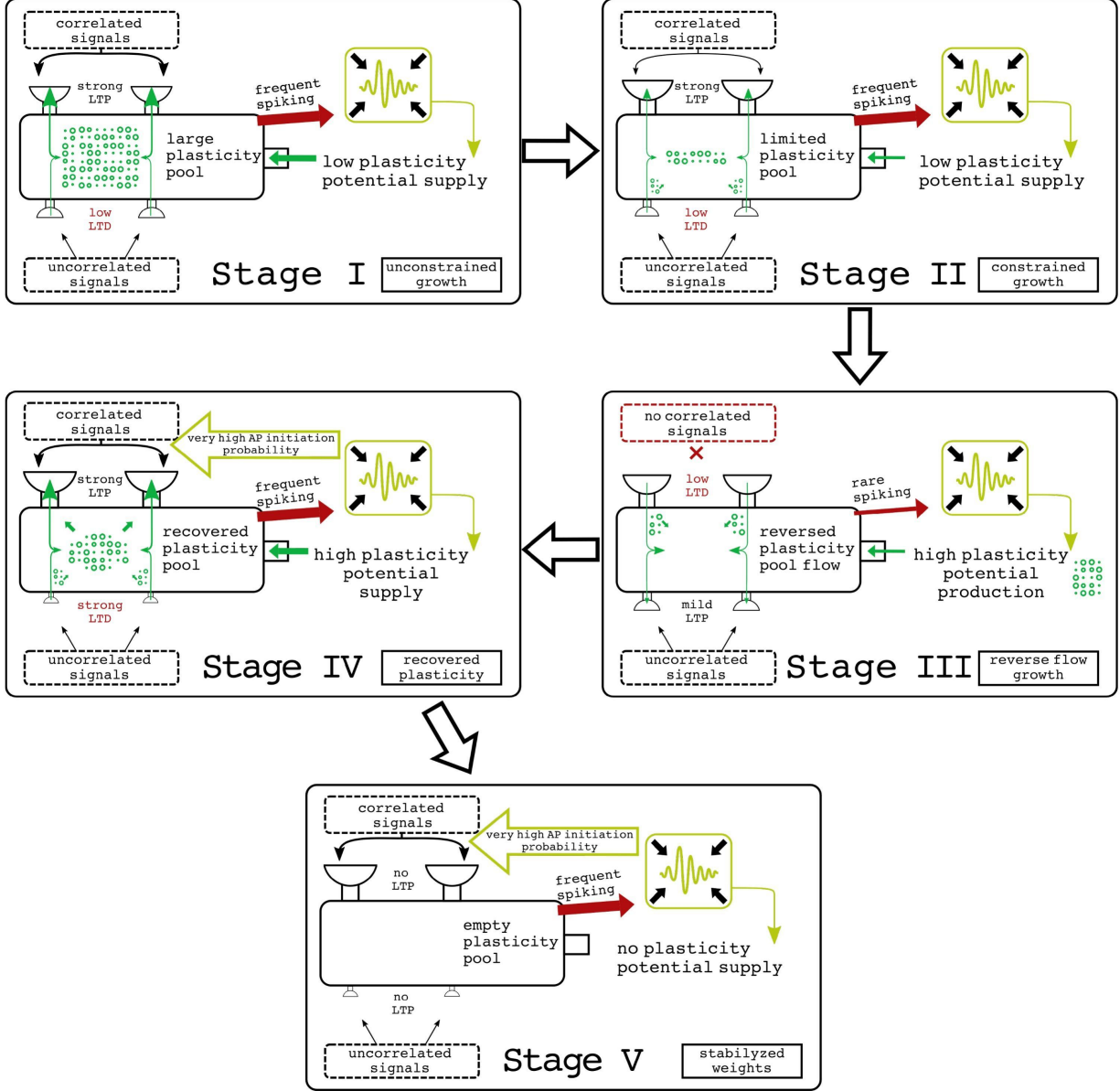


Figure 6: One proposed scenario for weight control and dynamics in the model.

where w_d^{res} is the maximum amplitude of growth of the sum of weights on the dendrite d in t previous steps.

$$k_{soma}^{sat} = 1 + \left(\frac{w_{soma}^{pool}}{\sum_d \Delta w_d^{pool}} - 1 \right) \cdot H(\sum_d \Delta w_d^{pool} - w_{soma}^{pool}), \quad (22)$$

where w_{soma}^{pool} is the global reserve of the plasticity potential, and it's dynamics is calculated as follows:

$$\dot{w}_{soma}^{pool} = w_{soma}^{pool} - k_{soma}^{sat} \cdot r^{speed} \cdot \sum_d \Delta w_d^{pool}. \quad (23)$$

There are constant parameters in the model: $r^{siss} = 0.1$, $k_{back} = 0.2$, $w_{ds}^{ideal} = 0.5$.

Figure 6 reflects the desired dynamics in the one particular dendrite with weights, restricted by plasticity potential reserve. Before the process of stimulation, all weights on the dendrite are equal. But then, part of them stimulated with random independent noise and another part with correlated input signals. It will lead to the increase of spiking activity of a neuron (Figure 6, Stage I). As there is a lot of weight growth potential in the dendrite, nothing prevents weights to grow according to the STDP rule and some synapses with correlated activity will initiate a strong LTP and those with uncorrelated will experience mild LTD. In response to the increased firing rate plasticity potential reserve, the control system will reduce plasticity materials release. This will lead to the next stage (Figure 6, Stage II). At this stage weight growth is constrained by the limited reserve of plasticity potential materials. It will lead to the growth of correlated stimulated synapses at the expense of shrinking others.

If correlated input stops (Figure 6, Stage III), synapses, that have at least some uncorrelated input will grow at the expense of decreasing previously outgrown synapses. As the neuron will start only receiving random uncorrelated noise, this will lead to a decrease in spiking frequency and the control system will release more plasticity potential materials. It will be delivered to dendrite and after the recovery of correlated input, synapses, receiving that input will grow to the point when they will initiate action potentials without any random co-stimulation. This will lead to strong divergence in synaptic weights of correlated and uncorrelated inputs. A strong reaction to correlated inputs will initiate strong firing output, which will lead again to the interruption of plasticity potential materials reserve. If all plasticity potential materials and input signals will persist on the same level, the synaptic weights will stabilize due to spike-independent synaptic scaling (SISS) at the dendrite (Figure 6, Stage V).

The described weight dynamics restricted by plasticity potential materials reserve should lead to higher weight divergence between correlated and uncorrelated inputs and will also eventually settle weights on some 'saddle points'.

Note that we can regulate the filtering of synaptic noise by manipulating with target firing rate. If the target frequency θ_{target} is high, the neuron will act as a basic STDP and will allow synapses to easily develop. While at low θ_{target} , it will let to develop only synapses with strongly correlated and limited frequencies.

So we describe all necessary parts of our proposed framework, such as the basic plasticity rule, the spiking behavior, the dynamics of synaptic plasticity potential storage, and the overall paradigm of its regulation. In the next section, we introduce the particular control approaches that we use in the present paper for the regulation of plasticity potential storage in the neuron and its dendrites.

2.5 Models of plasticity potential reserve control

Thus, we use the following algorithm of the neuron plasticity regulation model. (Algorithm 1)

Algorithm 1: Neuron plasticity regulation model

Require: I_{ds}

- 1: Calculate integrated weighted input I to the neuron (Equations 5–6)
 - 2: Generate the integrated output O from the spiking model (Equation 7)
 - 3: Update Δw_{ds}^{stdp} (Equations 1–2)
 - 4: Recalculate Δw_{ds}^{stdp} (Equations 12–13) based on the availability of plasticity potential in each dendrite (w_d^{pool}) and finally update w_{ds} (Equations 11)
 - 5: Set the new state of the plasticity potential reserve w_{soma}^{pool} (particular implementations of control approaches are described in Section 2.5) with respect to firing frequency θ_{real} control
 - 6: Update w_d^{pool} based on the new w_{soma}^{pool} (Equations 17–23)
 - 7: **return** New step
-

At first, in neuron synapses receive inputs in the form of '0' and '1', where '0' means that no signal is received, and '1' – is the received signal. Inputs I_{ds} are multiplied by the weights w_{ds} , and then scaled and directed to the spiking model. Based on the timing between inputs and action potential generation (O), update for weights, Δw_{ds}^{stdp} is calculated. After that, the weight growth is regulated by a control mechanism. In our case, we test and compare three different kinds of control algorithms, described in Sections 2.5.1–2.5.3:

1. firing frequency-dependent allocation model,
2. echo state network (ESN) control,
3. backward calculation of plasticity potential reserve demand.

Table 1: Proposed Q -learning parameters for ESN

Parameters	Values
State	$w_d^{pool}, w_{ds}, \theta_{real}$
Actions	$w_{soma}^{pool} = 0$ or $w_{soma}^{pool} = \sum_d w_d^{res}$
Q -values	Divergence from θ_{target} level

Plasticity potential reserve (w_{soma}^{pool}) is assigned by one of three algorithms. Plasticity potential reserve in dendrites w_d^{pool} is then refilled from w_{soma}^{pool} . The w_d^{pool} determines the ability of weights in particular dendrite to grow according to STDP weight update and we get the final weights after the one loop cycle.

Therefore, this algorithm of neuron plasticity regulation describes the processes in the abstract neuron including the change in the synaptic weights and control of the plasticity potential reserve. Below we describe three w_{soma}^{pool} control algorithms.

2.5.1 Firing frequency-dependent allocation model

Firing frequency-dependent allocation model represents the restriction mechanism when if the firing frequency θ_{real} is less than the target frequency θ_{target} , then the plasticity potential reserve in soma w_{soma}^{pool} is assigned in accordance with the difference between these frequencies (Equation 24).

$$w_{soma}^{pool} = \begin{cases} \sum_d w_d^{res} \cdot (\theta_{target} - \theta_{real}), & \text{if } \theta_{real} < \theta_{target} \\ 0, & \text{otherwise} \end{cases} \quad (24)$$

When θ_{real} is not enough to reach the target frequency θ_{target} , then we begin to add the plasticity potential to prevent θ_{real} from falling below the target.

2.5.2 ESN control

The approach from the Section 2.5.1 should be tuned by hands for each neural structure such as a number of s and d and to the task input intensity. Hence, it cannot be applied to complex tasks and networks where we do not know these parameters. It is provided more like a demonstration of an approach. For more complex tasks we need to control w_{soma}^{pool} by some sort of adaptive algorithm. It might be either the black box kind of control system or the direct numeric calculation of optimal w_{soma}^{pool} . Here, we provide the approach to regulation of weight potential reserve by ESN network as inspired by cellular GRN/PPI networks approach with universal computing capabilities. We train it with reinforcement learning as it is hard to calculate the exact teaching labeling for training in our setup.

Genetic regulation is a non-linear dynamic information processing that occurs in the network structure and has a complex interaction graph consisting of the work of GRN and protein interactions. Modeling of genetic regulatory networks of cells using ESN has been proposed in [6].

ESN in the task of reinforcement learning was proposed in [46] and consists of adapted SARSA Q -learning, where ESN is used to approximate the action-state pairs. We also propose to use the ESN for the creation of an adapted Q -learning system [47] for dynamic optimization of the neuron parameters. (Table 1)

Intraneural ESN-network controls w_{soma}^{pool} during the Q -learning, thus, constraining the growth of synaptic weights. The neuron is trying to optimize the firing frequency level θ_{real} . The level of the plasticity potential (w_{soma}^{pool}) was controlled by ESN giving two options of actions: provide the w_{soma}^{pool} to dendrites or not. Internal values are controlled by neuronal ESN reinforcement learning.

Our ESN consists of two input layers, the reservoir size is 25, the contraction coefficient is 0.9, the density is 1.0, and the scale input coefficient is 1.0, $\gamma = 0.4$, $\epsilon = 0.05$, and it gradually decreases to 0.005 by the last step.

The reward for ESN is calculated as:

$$R = |\theta_{target} - \theta_{real}| \cdot k^{rew}, \quad (25)$$

where k^{rew} is the reward scaling coefficient, here, $k^{rew} = -10$.

2.5.3 Backward calculation of plasticity potential reserve demand

If we consider that future inputs to the neurons might be sampled based on the known history of previous inputs then we may assume the future STDP weight change and demand across all the synapses and calculate the exact amount of w_{soma}^{pool} that should be injected into the model to shift the firing frequency of a neuron towards the desired value θ_{target} . This cannot be done with ideal precision, but if assumptions and calculation will be done each step it should drive the frequency towards an optimal firing frequency state.

We propose an algorithm to control the firing frequency by calculating the global reserve of the plasticity potential w_{soma}^{pool} and correcting it. (Algorithm 2)

Algorithm 2: Control of firing frequency based on w_{soma}^{pool} allocation by direct demand calculation

Require: I_{ds}, θ_{target}

- 1: Calculate w_{ds}^{min} (if $w_d^{pool} = 0$) and w_{ds}^{max} (if $w_d^{pool} = w_d^{res}$)
 - 2: Calculate θ_{input}^{t-wind}
 - 3: Calculate I_{ds}^{t+wind} using sampling I_{ds}^{t-wind} with θ_{input}^{t-wind} and Bernoulli distribution
 - 4: Calculate $I_{ds}^{t+wind} \cdot w_{ds}^{min}$ and $I_{ds}^{t+wind} \cdot w_{ds}^{max}$
 - 5: Get θ_{min} and θ_{max} from the Equations 3–4
 - 6: Compare with θ_{target} :
 - 7: **if** $\theta_{target} < \theta_{min}$ **then**
 - 8: Set $w_{soma}^{pool} = 0$
 - 9: **else if** $\theta_{target} > \theta_{max}$ **then**
 - 10: Set $w_{soma}^{pool} = w_d^{res}$
 - 11: **else if** $\theta_{min} \leq \theta_{target} \leq \theta_{max}$ **then**
 - 12: Calculate w_{soma}^{pool} using the Equations 26–30
 - 13: **end if**
 - 14: **return** w_{soma}^{pool}
-

For this, the required frequency θ_{target} is set. Then, the theoretically possible minimum w_{ds}^{min} (if w_d^{pool} is equal to zero) and maximum w_{ds}^{max} (if w_d^{pool} is maximum possible) values of the weights are calculated. After that, the estimated inputs I_{ds}^{t+wind} for a given forward window $wind$ are calculated: the frequency of inputs θ_{input}^{t-wind} for the $(t - wind)$ time steps (backward window) is calculated and the inputs I_{ds}^{t-wind} or the $(t - wind)$ time steps are sampled with the received frequency θ_{input}^{t-wind} and Bernoulli distribution. The estimated inputs I_{ds}^{t+wind} are multiplied by the corresponding weights and put into the spiking model (from the Equations 3–4), resulting in the estimated θ_{min} and θ_{max} frequencies.

We compare the obtained frequencies with a given frequency θ_{target} : if θ_{target} is less than θ_{min} , then we zero the w_{soma}^{pool} , if it is greater than θ_{max} , then we take w_{soma}^{pool} equal to the maximum possible value w_d^{res} , if it is in the interval between them, then we calculate w_{soma}^{pool} using backward calculation (the Equations 26–30):

$$w_{soma}^{pool} = \sum_d \left(\frac{\sum_d \Delta w_d^{pool} \cdot (\dot{w}_d^{pool} - w_d^{pool} + \sum_s \Delta w_{ds}^- + k_d^{sat} \cdot \sum_s \Delta w_{ds}^+ - (1 - H_{soma}^{wp}) \cdot \Delta w_d^{pool} \cdot r^{speed})}{\Delta w_d^{pool} \cdot r^{speed} \cdot H_{soma}^{wp}} \right), \quad (26)$$

where

$$H_{soma}^{wp} = H(\sum_d \Delta w_d^{pool} - w_{soma}^{pool}), \quad (27)$$

$$\dot{w}_d^{pool} = \sum_s \left(\frac{\sum_s \Delta w_{ds}^{stdp+} \cdot (\dot{w}_{ds}^{new} - k_d^{siss} \cdot (w_{ds} + \Delta w_{ds}^{stdp} \cdot (1 - H_d^{wp})))}{\Delta w_{ds}^{stdp} \cdot H_d^{wp}} \right), \quad (28)$$

where

$$H_d^{wp} = H\left(\sum_s \Delta w_{ds}^{stdp+} - \frac{w_d^{pool}}{k_d^{siss}}\right) \cdot H(\Delta w_{ds}^{stdp}), \quad (29)$$

$$\dot{w}_{ds}^{new} = w_{ds}^{min} + (w_{ds}^{max} - w_{ds}^{min}) \cdot \frac{(\theta_{target} - \theta_{min})}{(\theta_{max} - \theta_{min})}, \quad (30)$$

where w_{ds}^{min} and w_{ds}^{max} are the minimum and the maximum value of the synaptic weights; θ_{target} , θ_{min} , and θ_{max} denote the target, the minimum and the maximum firing frequency.

Above we provided four kinds of approaches of restricting weight outgrowth based on keeping firing frequency goal. These approaches should be tested for reaction on different kinds of synaptic input simulation resembling some regimes that might emerge in spiking neural networks. These models will be compared to the performance of the basic STDP weight update rule. The next section covers such testing.

3 Results

To explore the approaches described above, we run a series of experiments comparing the following weight outgrowth restriction models (as well as the basic STDP weight update rule model):

1. basic STDP weight update rule (Equations 1–2);
2. homeostatic synaptic scaling (HSS);
3. firing frequency-dependent allocation (FFDA);
4. echo state network (ESN) control;
5. backward calculation of plasticity potential reserve demand (PPD).

In all experiments, the same inputs are given for all types of models. In various experiments, depending on the task, either low-frequency ($\theta_{target} = 0.2$) or high-frequency ($\theta_{target} = 0.5$) inputs are used. Also, all experiments are carried out on one neuron, 3 dendrites, 6 synapses. Each experiment takes 2400 steps and 100 such tests are performed for each task. The results for 100 tests are averaged for display on figures, excluding figures for inputs and spiking.

Two setups, except for the experiments with correlated inputs, are compared: with spiking independent synaptic scaling (SISS) in the model or not.

The presented modeling results contain such indicators as: input, input frequency, spiking O , spiking frequency θ_{real} , w_{ds} and w_d^{pool} for all and each dendrites, w_{soma}^{pool} . Below, the results of experiments with 4 different protocols are presented.

3.1 Experiments

The experimental protocols for comparing the models with different approaches described above are following:

1. constant stimulation;
2. discrete neuron-wise high-frequency perturbations;
3. discrete dendrite-specific high-frequency perturbations;
4. experiments with correlated inputs.

3.1.1 Constant stimulation

In the present paper, we test the dynamics of different kinds of frequency homeostasis based algorithms of weight plasticity control. First, the saturation of weights should be tested. All synapses of all dendrites receive inputs with a constant frequency ($\theta_{input} = 0.2$). Thus, there is constant stimulation of the neuron. This is the simplest experiment that allows us to study the performance of the system in a stable environment without disturbances. (Figure 7)

The basic STDP, homeostatic synaptic scaling (HSS), and two approaches to the weight regulation based on plasticity potential reserve control (firing frequency-dependent allocation (FFDA) and backward calculation of plasticity potential reserve demand (PPD)) are presented in Figure 7. Test with and without spiking independent synaptic scaling (SISS) is shown. In Figure 7C the heatmap for all synaptic weights for all the algorithms provided. It can be seen that with pure STDP synaptic weights do grow to high values. SISS keeps those values lower because it constantly counteracts against the weights' extensive growth towards the goal point of dendritic weights $\sum_s w_{ds}^{ideal}$. Firing-rate homeostasis models do

a better job at keeping from weight outgrowth. HSS and PPD efficiently keep weights on medium values and firing rate θ_{real} close to target value θ_{target} . At the same time, simple equation-based approach FFDA overcompensates against weight growth and drive firing rate too low. To further test the algorithm more complex experiments are needed.

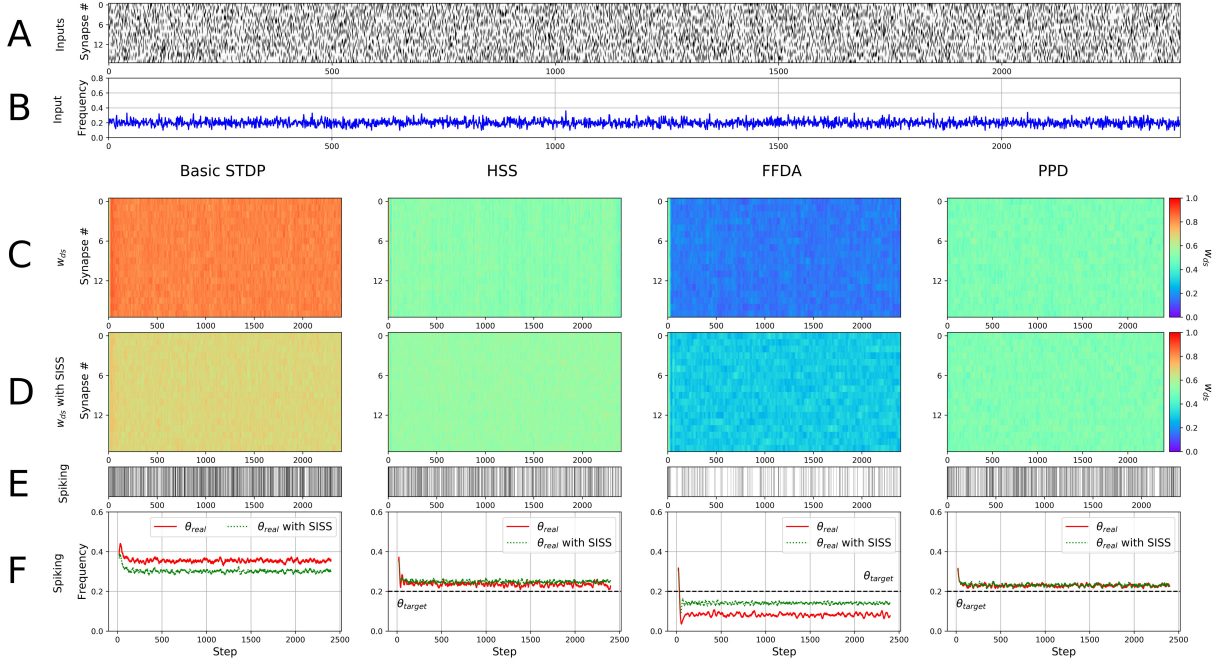


Figure 7: Constant stimulation experiment. All parameters in graphs in the figure are calculated for 2400 steps each of the basic STDP, HSS, FFDA, and PPD models, respectively, and averaged for all synapses and dendrites over 100 tests for each model (except (A), (E), are the non-averaged examples from the last test). (A) Inputs arrive at all synapses with constant frequency ($\theta_{input} = 0.2$) equal for all models. (B) Input frequency. (C) Dynamics of the synaptic weights w_{ds} without SISS, where the color indicates the w_{ds} value. (D) Dynamics of the synaptic weights w_{ds} with SISS, where the color indicates the w_{ds} value. (E) Action potential generation (spiking) O of the neuron ('0' and '1' values) during the work of the models. (F) Spiking frequency θ_{real} with and without SISS and level of target frequency θ_{target} .

3.1.2 Discrete neuron-wise high-frequency perturbations

To test the dynamics of weight control reaction to different inputs, experiment with discrete neuron-wise high-frequency perturbations are carried out, where all synapses of all dendrites of a neuron continually receive low-frequency inputs ($\theta_{input} = 0.2$), but from 600 to 1000 steps and from 1600 to 2000 steps the frequency of inputs changes to $\theta_{input} = 0.5$. Thus, at the moments of frequency change, high-frequency inputs received by the model, which can be compared with disturbances in the input signal of the neuron and impose an additional need on the system to regulate this process. Basic STDP and three approaches to plasticity potential reserve control are tested. We do it to find out how efficient are algorithms proposed in the paper above. (Figure 8)

In Figure 8 it can be seen that in contrast to STDP all weight restricting approaches lead to the decrease of more frequent input weights. This is because weight increase drives neurons out of firing frequency homeostatic state. We can also see that with no SISS FFDA and ESN based approaches fail to stabilize firing frequency and slowly decrease it, but despite this fact they react to firing frequency jumps. FFDA and ESN overcompensate the weight limitations. Only PPD is correct in control. SISS upregulation stabilizes the control of θ_{target} .

In this section, we prove that plasticity potential reserve control approaches do function in practice and we may choose one for future testing and practice use. Given the complexity of tuning, control quality and computing cost using ESN for control are unfavorable. But neuron model for this paper includes different dendrites. In the next section, we test how proposed algorithms will act in a more non-linear setup.

3.1.3 Discrete dendrite-specific high-frequency perturbations

To test the dynamics of weights between different dendrites it is necessary to provide dendrites with different input intensities. That is why the signals are applied selectively to different synapses.

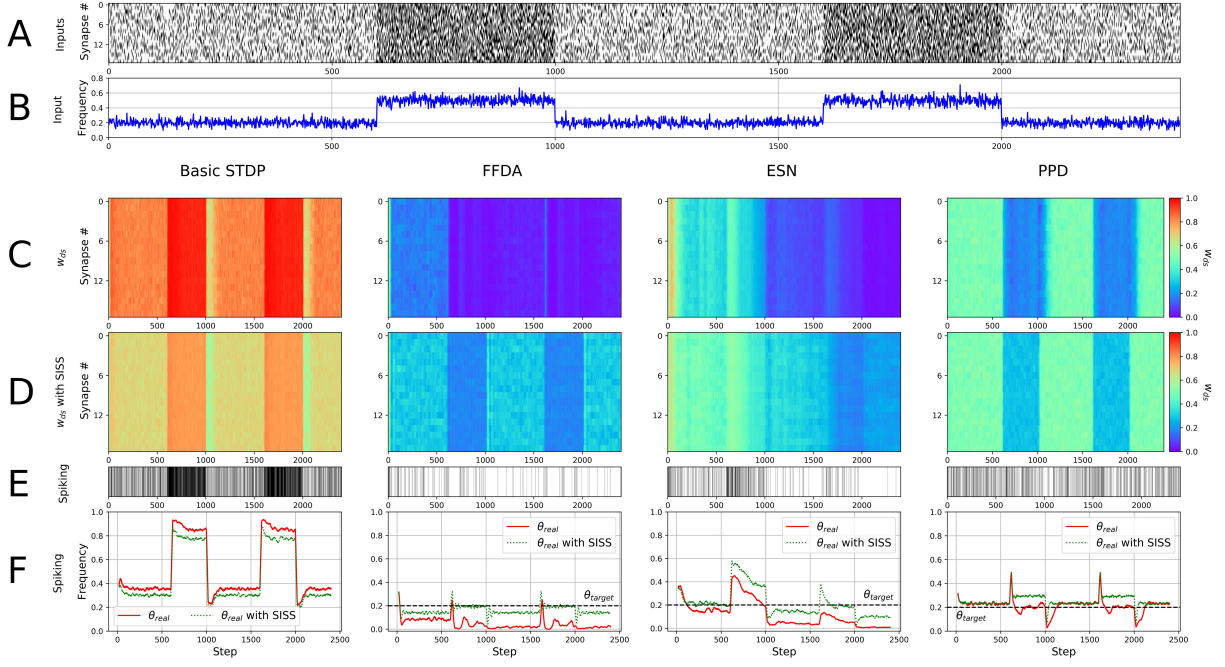


Figure 8: The results of the experiment with discrete neuron-wise high-frequency perturbations. All parameters in graphs in the figure are calculated for 2400 steps each of the basic STDP, FFDA, ESN, and PPD models, respectively, and averaged for all synapses and dendrites over 100 tests for each model (except (A), (E), are the non-averaged examples from the last test). (A) Inputs with frequency $\theta_{input} = 0.2$ equal for all models arrive at all synapses, but from 600 to 1000 steps and from 1600 to 2000 steps the frequency of inputs changes to $\theta_{input} = 0.5$. (B) Input frequency. (C) Dynamics of the synaptic weights w_{ds} without SISS, where the color indicates the w_{ds} value. (D) Dynamics of the synaptic weights w_{ds} with SISS, where the color indicates the w_{ds} value. (E) Action potential generation (spiking) O of the neuron ('0' and '1' values) during the work of the models. (F) Spiking frequency θ_{real} with and without SISS and level of target frequency θ_{target} .

The experiment with discrete dendrite-specific high-frequency perturbations is implemented as follows: all synapses of the first dendrite, four synapses of the second dendrite and two synapses of the third dendrite receive low-frequency inputs ($\theta_{input} = 0.2$), while two synapses of the second dendrite and four synapses of the third dendrite receive from 600 to 1000 steps and from 1600 to 2000 steps high-frequency inputs ($\theta_{input} = 0.5$). All the rest of the time, except for these steps, the last ones also receive low-frequency inputs. Thus, this experiment repeats the previous (the second) one, but in this case the input frequency vary depending on the dendrites. (Figure 9)

Figure 10 shows the changes in the plasticity potential reserve in dendrites w_d^{pool} for each dendrite and the global reserve of the plasticity potential w_{soma}^{pool} of three models - FFDA, ESN, PPD. And each graph compares two types of w_d^{pool} - with SISS and without it.

The HSS reduces the weights at the synapses to approach the target frequency. (Figure 9) It manages to adhere to the target frequency during periods with high-frequency inputs. At the same time, it can be seen that the weights change simultaneously on all dendrites, including on the first dendrite, 6 of its synapses do not receive a high-frequency input. SISS in HSS does not allow to reduce the weights during these intervals to the desired degree, and the HSS itself cannot redistribute the weights at synapses. As a result, the spiking frequency in these intervals rises above the target.

In both cases (with and without SISS) FFDA decreases in weights at all synapses, but with SISS they do not fall so low, because it restrains them. Moreover, when there is a SISS, a redistribution of weights occurs to an insignificant extent. Synapses with high-frequency inputs decrease weights, due to this, weights increase at synapses with low frequencies located on the same dendrites. The θ_{real} is below the θ_{target} , while, due to the SISS, the θ_{real} for this case is closer to the θ_{target} . The Figure 10D of w_{soma}^{pool} shows that in cases with SISS, a decrease in weights is suppressed in comparison with the model without SISS, therefore, it can be seen that w_d^{pool} for the case with SISS arrive into dendrites very few.

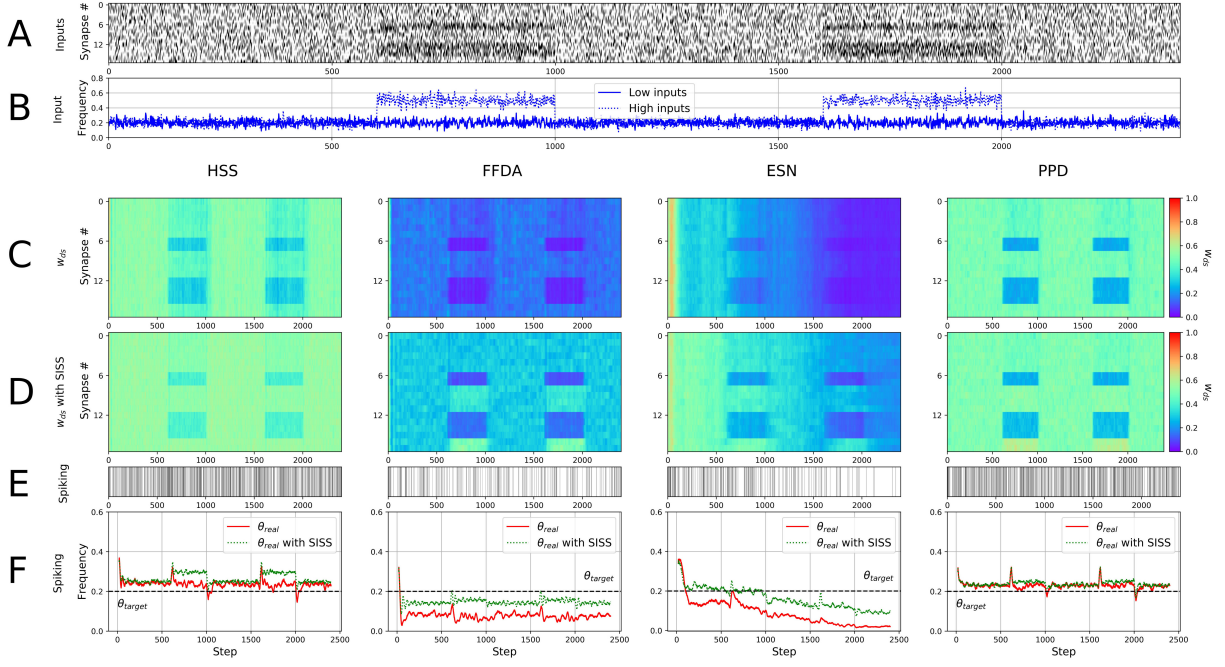


Figure 9: The results of the experiment with discrete dendrite-specific high-frequency perturbations. All parameters in graphs in the figure are calculated for 2400 steps each of the HSS, FFDA, ESN, and PPD models, respectively, and averaged for all synapses and dendrites over 100 tests for each model (except (A), (E), which are the non-averaged examples from the last test). (A) Inputs with frequency $\theta_{input} = 0.2$ equal for all models arrive at all synapses of the 1st dendrite, 4 synapses of the 2nd dendrite and 2 synapses of the 3rd dendrite, while at 2 synapses of the 2nd dendrite and 4 synapses of the 3rd dendrite from 600 to 1000 steps and from 1600 to 2000 steps arrive high-frequency inputs ($\theta_{input} = 0.5$). (B) Input frequency, where 'Low inputs' and 'High inputs' are low-frequency and high-frequency inputs, respectively. (C) Dynamics of the synaptic weights w_{ds} without SISS, where the color indicates the w_{ds} value. (D) Dynamics of the synaptic weights w_{ds} with SISS, where the color indicates the w_{ds} value. (E) Action potential generation (spiking) O of the neuron ('0' and '1' values) during the work of the models. (F) Spiking frequency θ_{real} with and without SISS and level of target frequency θ_{target} .

For the FFDA without SISS, w_{soma}^{pool} was also restricted, however, w_d^{pool} has sufficient reserve, which is not consumed due to rare spikes.

At the first steps in the ESN, the weights at the synapses are raised, due to this, the θ_{real} is higher than the θ_{target} . After that, the ESN is trained to reduce the weights and by the time the first interval with high-frequency inputs begins, its spiking frequency is close to the target. After the end of this interval, the frequency of inputs decreases, and at the same time, the spiking frequency decreases. However, the model continues to adhere to the strategy of reducing the weights, showing its inability to overfit when the task conditions change. For the case without SISS, this strategy leads to such a significant reduction in weights that spiking almost stops after 2000 steps. In ESN with SISS, the process of weight reduction is more restrained, but the strategy itself does not change. Figure 10 clearly shows the strategy of decreasing w_{soma}^{pool} and the subsequent decrease of w_d^{pool} . At the same time, we see that for the case with SISS before the first interval with high-frequency inputs, the ESN successfully learned to increase w_{soma}^{pool} , however, after that, it could not return to this strategy.

In the PPD, during intervals of high-frequency inputs, the weights decrease to a greater extent at active synapses, while in the case of SISS, a more pronounced redistribution of weights occurs on the second and third dendrites. The PPD shows its effectiveness in achieving the target frequency, while with the SISS, there is no significant discrepancy between the θ_{real} and the θ_{target} . We see a stable strategy of setting w_{soma}^{pool} for all intervals with low-frequency inputs and boosting w_{soma}^{pool} for high-frequency intervals. For PPD with SISS, the w_{soma}^{pool} generation is more stable throughout the entire experiment.

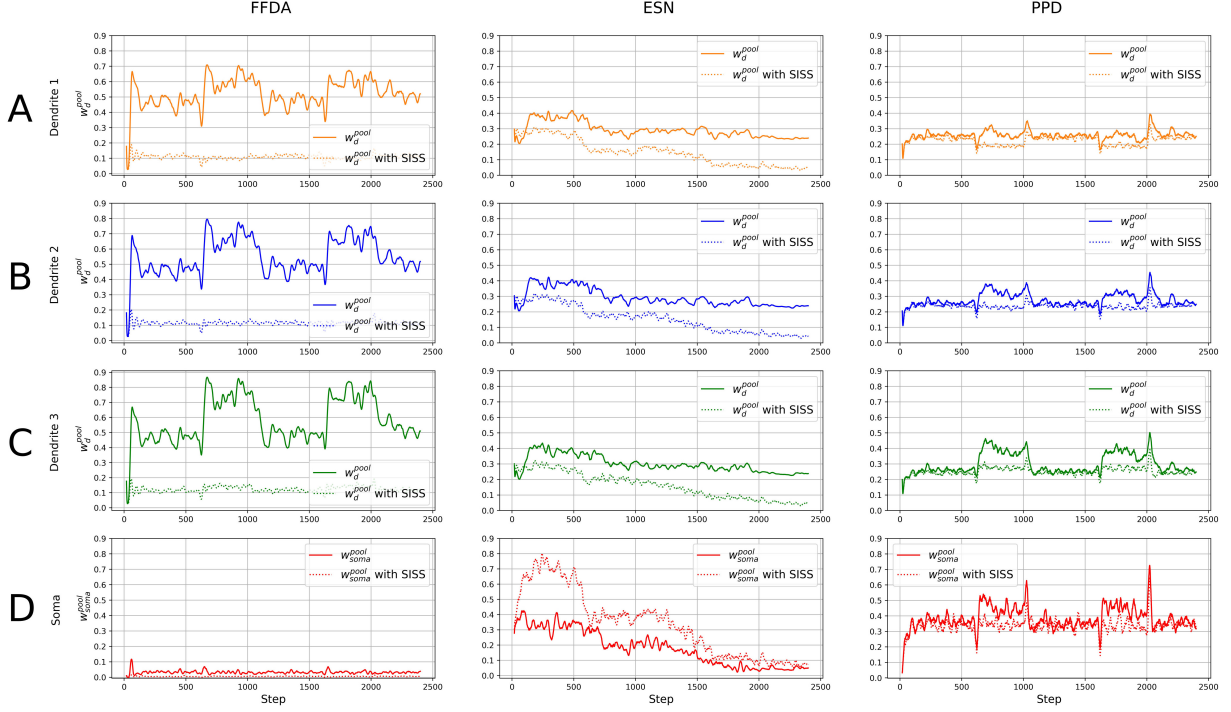


Figure 10: Comparison of the plasticity potential reserve in dendrites for each dendrite and the global reserve of the plasticity potential of three models: FFDA, ESN, PPD. All parameters in graphs in the figure are calculated for 2400 steps each of the FFDA, ESN, and PPD models, respectively, and averaged for all synapses and dendrites over 100 tests for each model. (A)-(C) Dynamics of the plasticity potential reserve in dendrites w_d^{pool} with and without SISS on the 1st, 2nd and 3rd dendrites, respectively. (D) Dynamics of global reserve of the plasticity potential w_{soma}^{pool} with and without SISS.

It could be concluded from the current experiment that homeostatic frequency control approaches have filtered disturbing high-frequency inputs. FFDA and ESN can successfully signal discrimination only of the presence of SISS while HSS and PPD can adaptively filter with no additional mechanisms. PPD not only filtered high-frequency input noise but has also heterosynaptically upscaled inputs with low frequencies in presence of SISS. PPD with SISS performs the best as a self-learning filter on the particular task.

3.1.4 Experiments with correlated inputs

Local learning rules in spiking neural networks, such as STDP are desired to find correlations in the data. Indeed the original Hebb's postulate stating: "fire together - wire together" means that it should be a correlation between the presynaptic stimulus and postsynaptic output. That is why it is most important to find out, how STDP and its constrained versions (HSS and plasticity reserve-based approach) react on correlated signals. We also compare the reactions to the intense input with high frequency and high-correlated input. As we have seen above, high-frequency input leads to weight degradation. But coincidental arrival rate of frequent and correlated inputs should be similar and this points that it is important to study such an interaction. Also, it is important for brain and artificial neural networks to keep a good signal-to-noise ratio when the stimulus is easily distinguishable from the background. This article is devoted to the frequency homeostatic models as it is important for neural network dynamics to keep the mean activation stable on the criticality edge. Below, we will inspect the plasticity control approaches with correlated stimulus protocol to test the models for their ability not only to respond to changes in the input frequency but also to distinguish between correlated inputs.

For this task, we use correlated inputs. We assume that some of the inputs are correlated. To create such inputs, we generate an initial 'mask' input. Then, we select synapses, which are set as correlated at certain time intervals. In this case, these are two synapses on the second dendrite and four synapses on the third dendrite (so that there are different numbers of correlated and uncorrelated inputs on different dendrites). After that, at the specified time intervals, when

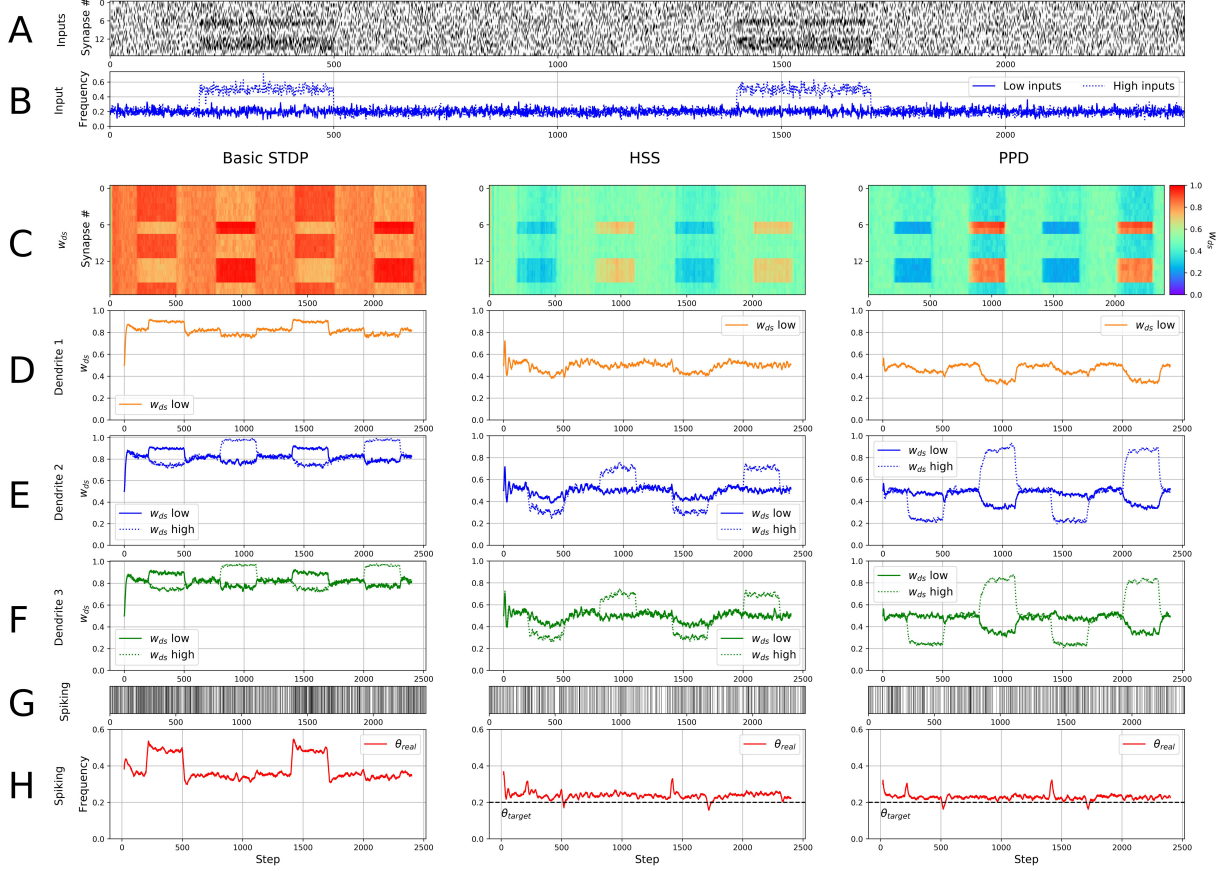


Figure 11: The results of the experiments with correlated inputs. All parameters in graphs in the figure are calculated for 2400 steps each of the basic STDP, HSS, and PPD models, respectively, and averaged for all synapses and dendrites over 100 tests for each model (except (A), (G), which are the non-averaged examples from the last test). (A) Inputs with frequency $\theta_{input} = 0.2$ arrive at all synapses of the 1st dendrite, 4 synapses of the 2nd dendrite, 2 synapses of the 3rd dendrite. The rest of the synapses (2 synapses of the 2nd dendrite and 4 synapses of the 3rd dendrite) receive the following inputs: from 200 to 500 steps and from 1400 to 1700 steps are high-frequency inputs ($\theta_{input} = 0.5$), and from 800 to 1100 steps and from 2000 to 2300 steps correlated signals are included with $\theta_{input} = 0.2$. (B) Input frequency, where 'Low inputs' and 'High inputs' are low-frequency and high-frequency inputs respectively. (C) Dynamics of the synaptic weights w_{ds} for all synapses and dendrites, where the color indicates the w_{ds} value. (D)-(F) Dynamics of the synaptic weights w_{ds} on the 1st, 2nd and 3rd dendrites respectively, ' w_{ds} high' are synaptic weights to which correlated signals are received, ' w_{ds} low' are synaptic weights to which correlated signals are not received. (G) Action potential generation (spiking) O of the neuron ('0' and '1' values) during the work of the models. (H) Spiking frequency θ_{real} and level of target frequency θ_{target} .

the correlated signal is turned on, these selected synapses, with a 90 percent probability for each of them, receive an input identical to the 'mask' input. In this experiment, we use correlated inputs, the correlation coefficient between which is very high (here it is 0.9). Thus, all synapses of the first dendrite, four synapses of the second dendrite, two synapses of the third dendrite, as in the previous experiment, receive low-frequency inputs ($\theta_{input} = 0.2$), but two synapses of the second dendrite and four synapses of the third dendrite receive the following inputs: from 200 to 500 steps and from 1400 to 1700 steps are high-frequency inputs ($\theta_{input} = 0.5$), and from 800 to 1100 steps and from 2000 to 2300 steps are inputs with $\theta_{input} = 0.2$. Correlated signals are included at the same time intervals. (Figure 11)

Here we study and compare three models: the basic STDP, the homeostatic synaptic scaling (HSS) and the constrained plasticity potential reserve calculation controlled by direct demand (PPD). As can be seen by heatmaps of all weights (Figure 11C), all three models do react on frequent stimulus and correlated stimulus in opposite directions. Unlike frequent input, correlated input leads to strong LTP. The basic STDP model has the fastest reaction to signal time and weights stability of all the models. But it has no firing rate homeostasis. At the same time, both HSS and PPD models

Table 2: Values of the mean absolute error between ' w_{ds} low' and ' w_{ds} high'. STDP, HSS, PPD – compared models, LT – low target frequency, HT – high target frequency, LF – low input frequency, HF – high input frequency, FC – frequent/correlated task, DC – differently correlated task.

		STDP		HSS		PPD	
		LT	HT	LT	HT	LT	HT
FC	LF	0.20	0.19	0.20	0.19	0.46	0.23
	HF	0.06	0.07	0.05	0.03	0.18	0.06
DC	LF	0.19	-	0.19	-	0.46	-
	HF	0.15	-	0.13	-	0.23	-

do a good job at firing rate maintenance (Figure 11H). But HSS model does not provide any synaptic competition and heterosynaptic scaling phenomena. When the weights stimulated by correlated signal (' w_{ds} high') grow, weights with constant input (' w_{ds} low') are not affect (Figure 11D,E,F). In the case of PPD, we may see that the LTP of correlated synapses is accompanied by LTD in other synapses. At the same time, LTD of highly stimulated synapses does not affect other synapses' efficiency. This is different from HSS where LTD occurring in one synapse drives down others. This is important for the network activity that removal of one memory does not affect another but the introduction of new memories leads to higher specificity. In general, PPD has a much better signal-to-noise ratio for such a task. The divergence of differently stimulated versus stable synaptic weights during stimulation calculated as MAE was 0.46 for correlated periods and 0.23 for high-frequency stimulated (Table 2). The same values for HSS are 0.13 and 0.19 respectively. We may conclude about almost twice better signal specificity and more useful character of PPD weight dynamics based on this experiment.

Algorithms of keeping weight homeostasis such as PPD and HSS might be useful also for dynamic network frequency updates and local configuration. Firing-rate regulation might be used for dynamic coupling and efficient information transfer. Thus, it should be examined, how homeostatic frequency control approaches to weight restriction would behave with dynamic firing frequency θ_{target} and how much noise they will transfer with higher θ_{target} .

For this task, we administered some synapses at selected dendrites with correlated inputs of different intensities (high-frequency correlated signal and regular frequency). The synapse order repeats the previous experiment. We also changed the target frequency θ_{target} from low (0.2) to high (0.5) on two halves of experiment time.

The basic STDP model has increased all weights of correlated signals. At the same time, both HSS and PPD weight control algorithms filter even strong-correlated signal if it has a high frequency. But HSS disadvantage is low specificity because it penalizes all synapses. PPD approach instead penalizes only frequent signal and has stronger divergence.

At the high level of target frequency θ_{target} , both HSS and PDD start to react to both input frequencies (Figure 12D-F). Yet, regular correlated signals have stronger LTP than high-frequency ones. The target varying experiment shows the prevalence of the PPD approach over HSS in signal-to-noise ratios. We can see by heatmaps of weights (Figure 12C) that weight increase for a correlated signal during the high target period is more distinguishable. The MAEs for high-frequency and background inputs is 0.06 and for correlated and background is 0.23 for PPD given high the target. The same values for HSS are 0.03 and 0.19 (see Table 2). Both HSS and PPD started to react on noised input when set with high target frequency θ_{target} . It can be concluded that both algorithms are suitable for dynamic firing frequency control, but PPD better discriminates between signals.

4 Discussion

In the paper, we proposed the neuronal plasticity regulation model, which changes the potential synaptic weight growth by the control of the plasticity potential reserve to dynamically stabilize the artificial neuron activity. We described all parts of the proposed approach, such as the basic plasticity rule, the spiking behavior, the dynamics of synaptic plasticity potential reserve, and the overall paradigm of its regulation. The new control approaches for the regulation of plasticity potential storage in the neuron and its dendrites were introduced. We provided four kinds of approaches of restricting weight outgrowth based on keeping firing frequency goal. These approaches were tested for reaction on different kinds of synaptic input simulation resembling some regimes that might emerge in spiking neural networks. These models also were compared to the performance of the basic STDP weight update rule.

It was shown that a neuron can selectively respond to certain frequencies of input signals depending on the mode of plasticity potential production. An especially important feature of the model is that neuron with low-frequency target filters frequent coincident input while reacting to correlated signals. Neurons of this model are suitable for creating spiking neural networks and can be used for unsupervised training tasks even on modern neuromorphic hardware. The

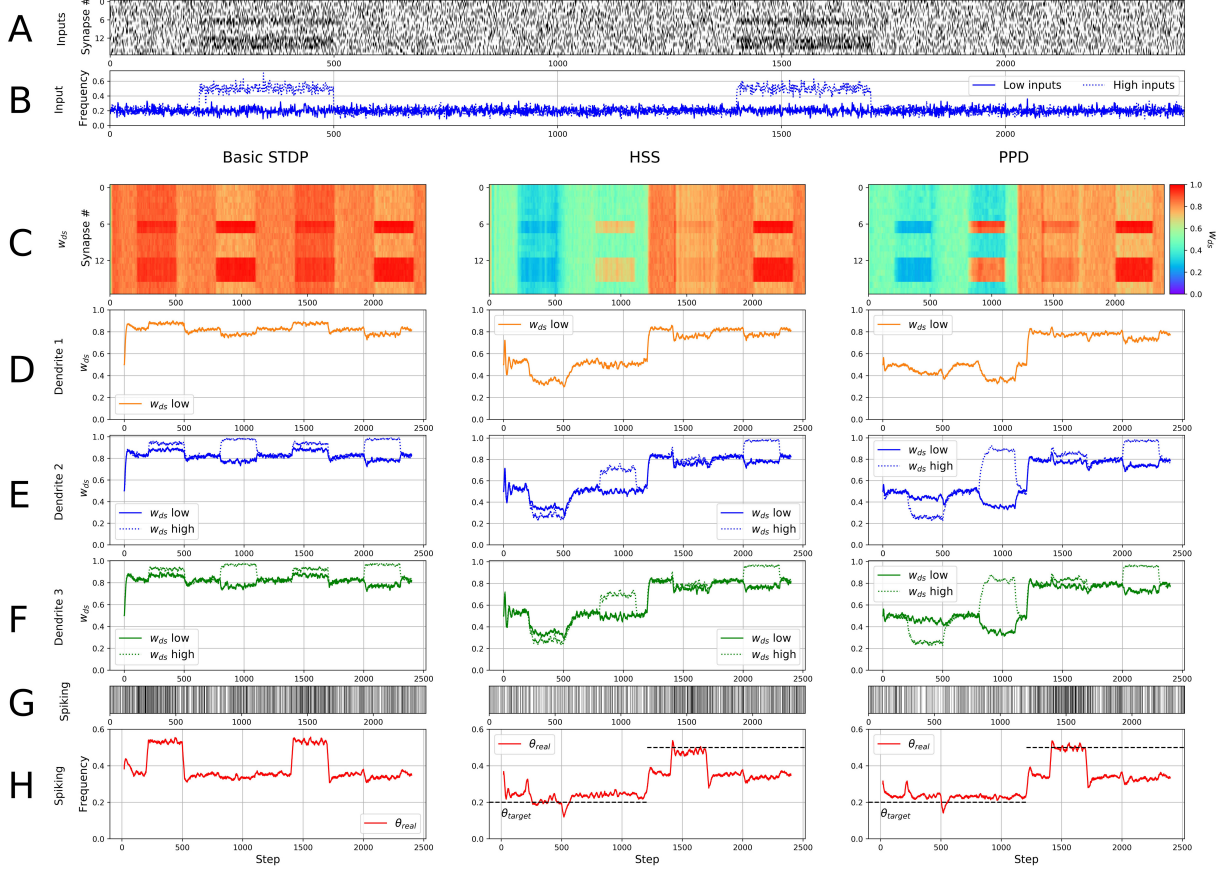


Figure 12: Correlated inputs experiments with changing target frequency θ_{target} . All parameters in graphs in the figure are calculated for 2400 steps each of the basic STDP, HSS, and PPD models, respectively, and averaged for all synapses and dendrites over 100 tests for each model (except (A), (G), which are the non-averaged examples from the last test). (A) Inputs with frequency $\theta_{input} = 0.2$ arrive at all synapses of the 1st dendrite, 4 synapses of the 2nd dendrite, 2 synapses of the 3rd dendrite. The rest of the synapses (2 synapses of the 2nd dendrite and 4 synapses of the 3rd dendrite) receive the following inputs: from 200 to 500 steps and from 1400 to 1700 steps are high-frequency inputs ($\theta_{input} = 0.5$) and correlated signals are included with $\theta_{input} = 0.5$, and from 800 to 1100 steps and from 2000 to 2300 steps correlated signals are included with $\theta_{input} = 0.2$. Target frequency from 1 to 1200 steps is 0.2, and from 1200 to 2400 steps it is 0.5. (B) Input frequency, where 'Low inputs' and 'High inputs' are low-frequency and high-frequency inputs respectively. (C) Dynamics of the synaptic weights w_{ds} for all synapses and dendrites, where the color indicates the w_{ds} value. (D)-(F) Dynamics of the synaptic weights w_{ds} on the 1st, 2nd and 3rd dendrites respectively, ' w_{ds} high' are synaptic weights to which correlated signals are received, ' w_{ds} low' are synaptic weights to which correlated signals are not received. (G) Action potential generation (spiking) O of the neuron ('0' and '1' values) during the work of the models; (H) Spiking frequency θ_{real} and level of target frequency θ_{target} .

implementations of STDP on memristors [48] allow limiting the weight growth in STDP by limiting the voltage-current application time. This resembles the dendritic plasticity potential reserve presented in the article.

Algorithms for homeostatic control of weights that take into account pre- and postsynaptic frequency, proposed in [49], maybe interesting for comparison with the model proposed in this article. Such approaches also lead to non-linear dynamics of weight restrictions, which highlights them from other homeostatic scaling techniques. But there are no reports on the heterosynaptic synaptic scaling in these papers. Heterosynaptic plasticity is implemented by Chen et al. [32]. But from the original paper, it seems that such a scaling prevents synaptic competition. The approach, presented in the current paper, particularly PPD, leads to heterosynaptic scaling, weights, and frequency-dependent homeostasis simultaneously. It is computationally effective and might be implemented not only for one neuron but for the entire layer, thus, reducing the overhead for computing optimal parameters.

Another important feature of the paper is its high signal-to-noise discrimination ability. This is very useful for many tasks for practical use in neural networks. Spiking neurons with PPD restricted STDP might be very useful for machine learning tasks.

For future research, it will be necessary to train the networks of neurons with such rules and to introduce some unsupervised learning methods. It might be also useful to find a way to regulate the firing frequency of neurons in the network to minimize the mean firing frequency in the network and to maximize the informational transfer. The free-energy principle [50] might be useful for this goal. Also, mutual information measures might be applied to tune SNN with PPD which will resemble real brain structures [51]. The casualty measures may help to obtain the optimal target frequencies for maximal important input-output network transfer [52]. In the future, we will also consider turning to a different spiking model because Izhikevich's is limited in firing frequency and it may be hard to obtain a correct spiking intercity for a given task.

Declaration of competing interest

The authors declare that they have no known competing financial interests or personal relationships that could have appeared to influence the work reported in this paper.

Acknowledgement

The computing resources of the Shared Facility Center "Data Center of FEB RAS" (Khabarovsk) were used to carry out calculations.

References

- [1] F. H. Sinz, X. Pitkow, J. Reimer, M. Bethge, and A. S. Tolias. Engineering a less artificial intelligence. *Neuron*, 103(6):967–979, 2019.
- [2] R. Kempter, W. Gerstner, and J. L. van Hemmen. Hebbian learning and spiking neurons. *Phys. Rev. E*, 59:4498–4514, 1999.
- [3] J. I. Castrillo, P. Pir, and S. G. Oliver. Yeast systems biology: Towards a systems understanding of regulation of eukaryotic networks in complex diseases and biotechnology. In A. J. M. Walhout, M. Vidal, and J. Dekker, editors, *Handbook of Systems Biology*, pages 343–365. Academic Press, San Diego, 2013.
- [4] B. Jones, D. Stekel, J. Rowe, and C. Fernando. Is there a liquid state machine in the bacterium *escherichia coli*? In *in Proceedings of the 2007 IEEE Symposium on Artificial Life (CI-ALife 2007)*, pages 187–191, 2007.
- [5] G. Tanaka, T. Yamane, J. B. Héroux, R. Nakane, N. Kanazawa, S. Takeda, H. Numata, D. Nakano, and Hirose A. Recent advances in physical reservoir computing: A review. *Neural Networks*, 115:100–123, 2019.
- [6] M. Gabalda-Sagarra, L. B. Carey, and J. Garcia-Ojalvo. Recurrence-based information processing in gene regulatory networks. *Chaos*, 115:106313, 2018.
- [7] W. Maass, T. Natschläger, and H. Markram. Real-time computing without stable states: A new framework for neural computation based on perturbations. *Neural Computation*, 14(11):2531–2560, 2002.
- [8] H. Jaeger and H. Haas. Harnessing nonlinearity: Predicting chaotic systems and saving energy in wireless communication. *Science*, 304(5667):78–80, 2004.
- [9] X. Dai. Is there a liquid state machine in the bacterium *escherichia coli*? In *in Advances in Neural Networks (ISNN 2004)*, pages 519–524, 2004.

- [10] A. Didovyk, O. I. Kanakov, M. V. Ivanchenko, J. Hasty, R. Huerta, and L. Tsimring. Distributed classifier based on genetically engineered bacterial cell cultures. *ACS Synthetic Biology*, 4(1):72–82, 2015.
- [11] S. Sinha, B. M. Jones, I. M. Traniello, S. A. Bukhari, M. S. Halfon, H. A. Hofmann, P. S. Katz, S. Huang, J. Keagy, V. J. Lynch, M. B. Sokolowski, L. J. Stubbs, S. Tabe-Bordbar, M. F. Wolfner, and G. E. Robinson. Behavior-related gene regulatory networks: A new level of organization in the brain. In *in Proceedings of the National Academy of Sciences*, volume 117, pages 23270–23279, 2020.
- [12] D. A. Jirenhed, A. Rasmussen, F. Johansson, and G. Hesslow. Learned response sequences in cerebellar purkinje cells. In *in Proceedings of the National Academy of Sciences of the United States of America*, volume 114, pages 6127–6132, 2017.
- [13] F. Johansson and G. Hesslow. Kir3 channel blockade in the cerebellar cortex suppresses performance of classically conditioned purkinje cell responses. *Scientific Reports*, 10(1):15654, 2020.
- [14] T. N. Grechenko. Conditioned inhibition of action potential generation in isolated helix pomatia neurons. *Neurosci. Behav. Physiol.*, 20(5):452–459, 1990.
- [15] A. L. Proskura, S. O. Vechkapova, T. A. Zapara, and A. S. Ratushnyak. Reconstruction of the molecular interactome of glutamatergic synapses. *Russ. J. Genet. Appl. Res.*, 5:616–625, 2015.
- [16] J. Kotaleski and K. Blackwell. Modelling the molecular mechanisms of synaptic plasticity using systems biology approaches. *Nature Reviews Neuroscience*, 11:239–251, 2010.
- [17] J. E. Pick and E. B. Ziff. Regulation of ampa receptor trafficking and exit from the endoplasmic reticulum. *Molecular and Cellular Neuroscience*, 91:3–9, 2010.
- [18] B. L. Tang. Nogo-a and the regulation of neurotransmitter receptors. *Neural Regeneration Research*, 15:2037, 2020.
- [19] A. Kempf and M. E. Schwab. Nogo-a represses anatomical and synaptic plasticity in the central nervous system. *Neural Regeneration Research*, 28(3):151–163, 2013.
- [20] K. Deisseroth, P. G. Mermelstein, H. Xia, and R. W. Tsien. Signaling from synapse to nucleus: the logic behind the mechanisms. *Current Opinion in Neurobiology*, 13(3):354–365, 2003.
- [21] P. Serrano, Y. Yao, and T. C. Sacktor. Persistent phosphorylation by protein kinase m ζ maintains late-phase long-term potentiation. *The Journal of Neuroscience*, 25(8):1979–1984, 2005.
- [22] S. F. Palida, M. T. Butko, J. T. Ngo, M. R. Mackey, L. A. Gross, M. H. Ellisman, and R. Y. Tsien. Pkm ζ , but not pkl λ , is rapidly synthesized and degraded at the neuronal synapse. *Journal of Neuroscience*, 35(20):7736–7749, 2015.
- [23] S. A. Korneev, D. V. Vavoulis, S. Naskar, V. E. Dyakonova, I. Kemenes, and G. Kemenes. A creb2-targeting microrna is required for long-term memory after single-trial learning. *Scientific Reports*, 8:3950, 2018.
- [24] J.-H. Han, S. A. Kushner, A. P. Yiu, C. J. Cole, A. Matynia, R. A. Brown, R. L. Neve, J. F. Guzowski, A. J. Silva, and S. A. Josselin. Neuronal competition and selection during memory formation. *Science*, 316(5823):457–460, 2007.
- [25] P. Sterling. Allostasis: A model of predictive regulation. *Physiology and Behavior*, 106(1):5–15, 2012.
- [26] F. Ali and A. C. Kwan. Interpreting in vivo calcium signals from neuronal cell bodies, axons, and dendrites: a review. *Neurophotonics*, 7(1):011402, 2020.
- [27] M. A. Brostrom and C. O. Brostrom. Calcium dynamics and endoplasmic reticular function in the regulation of protein synthesis: implications for cell growth and adaptability. *Cell Calcium*, 34(4-5):345–363, 2003.
- [28] L. Deng, Y. Wu, X. Hu, L. Liang, Y. Ding, G. Li, G. Zhao, P. Li, and Y. Xie. Rethinking the performance comparison between snns and anns. *Neural Netw.*, 121:294–307, 2020.
- [29] A. Masumori, T. Ikegami, and L. Sinapayen. Predictive coding as stimulus avoidance in spiking neural networks. In *IEEE Symposium Series on Computational Intelligence (SSCI), Xiamen, China*, pages 271–277, 2019.
- [30] R. Pascanu, T. Mikolov, and Y. Bengio. On the difficulty of training recurrent neural networks. volume 28, pages 1310–1318, 2013.
- [31] D. O. Hebb. *The organization of behavior: A neuropsychological theory*. John Wiley and Sons, Inc., New York, 1949.
- [32] J. Y. Chen, P. Lonjers, C. Lee, M. Chistiakova, M. Volgushev, and M. Bazhenov. Heterosynaptic plasticity prevents runaway synaptic dynamics. *Journal of Neuroscience*, 33(40):15915–15929, 2013.
- [33] G. G. Turrigiano. The self-tuning neuron: synaptic scaling of excitatory synapses. *Cell*, 135(3):422–435, 2008.

- [34] C.H. Bailey, M. Giustetto, Y.Y. Huang, R.D. Hawkins, and E.R. Kandel. Is heterosynaptic modulation essential for stabilizing hebbian plasticity and memory. *Nature Reviews Neuroscience*, 1(1):11–20, 2000.
- [35] M. C. W. Van Rossum, G. Q. Bi, and G. G. Turrigiano. Stable hebbian learning from spike timing-dependent plasticity. *Journal of Neuroscience*, 20(23):8812–8821, 2000.
- [36] F. Zenke, G. Hennequin, and W. Gerstner. Synaptic plasticity in neural networks needs homeostasis with a fast rate detector. *PLoS Comput. Biol.*, 9(11):e1003330, 2013.
- [37] M. Chistiakova, N. M. Bannon, M. Bazhenov, and M. Volgushev. Heterosynaptic plasticity: multiple mechanisms and multiple roles. *The Neuroscientist*, 20(5):483–498, 2014.
- [38] M. Kneussel and T. J. Hausrat. Postsynaptic neurotransmitter receptor reserve pools for synaptic potentiation. *Trends in Neurosciences*, 39(3):170–182, 2016.
- [39] G. Antunes and F. M. Simoes-de Souza. Ampa receptor trafficking and its role in heterosynaptic plasticity. *Scientific Reports*, 8:10349, 2018.
- [40] O. Nikitin and O. Lukyanova. Predictive regulation of neurotransmitter receptor pool for weight correction restriction. *Procedia Computer Science*, 145C:393–399, 2018.
- [41] O. Nikitin and O. Lukyanova. Homeostatic neural network for adaptive control: Examination and comparison. *Lecture Notes in Computer Science*, 10994:223–235, 2018.
- [42] E. M. Izhikevich. Simple model of spiking neurons. *IEEE Transactions on Neural Networks*, 14(6):1569–1572, 2003.
- [43] S. Song, K. D. Miller, and L. F. Abbott. Competitive hebbian learning through spike-timing dependent synaptic plasticity. *Nature Neuroscience*, 3:919–926, 2000.
- [44] C. Gonzalez-Islas, P. Bülow, and P. Wenner. Regulation of synaptic scaling by action potential-independent miniature neurotransmission. *Journal of neuroscience research*, 96(3):348–353, 2018.
- [45] Mf. Fong, J. P. Newman, S. M. Potter, and P. Wenner. Upward synaptic scaling is dependent on neurotransmission rather than spiking. *Nat Commun*, 6:6339, 2015.
- [46] I. Szita, V. Gyenes, and A. Lörincz. Reinforcement learning with echo state networks. In *Artificial Neural Networks – ICANN 2006*, volume 4131, pages 830–839, 2006.
- [47] C.J.C.H. Watkins and P. Dayan. Q-learning. *Mach Learn*, 8:279–292, 1992.
- [48] S. Yao, P. Xinqiang, and Xiangyu S. *Spike-Timing-Dependent Plasticity in Memristors*. Alex Pappachen James, IntechOpen, 2017.
- [49] J. K. Liu. Learning rule of homeostatic synaptic scaling: Presynaptic dependent or not. *Neural Computation*, 23:3145–3161, 2011.
- [50] K. Friston, J. Kilner, and L. Harrison. A free energy principle for the brain. *Journal of Physiology*, 100(1-3):70–87, 2006.
- [51] N. Schweighofer, K. Doya, H. Fukai, J. V. Chiron, T. Furukawa, and M. Kawato. Chaos may enhance information transmission in the inferior olive. *Proc Natl Acad Sci U S A*, 101(13):4655–4660, 2004.
- [52] A. K. Seth and G. M. Edelman. Distinguishing causal interactions in neural populations. *Neural Computation*, 19(4):910–933, 2007.